Supporting Information

2D MoS_2 nanosheets on 1D anodic TiO_2 nanotube layers: efficient co-catalyst for liquid and gas phase photocatalysis

Martin Motola, [a] Michal Baudys, [b] Raul Zazpe, [ac], Miloš Krbal,[a] Jan Michalička,[c] Jhonatan Rodriguez-Pereira,[a] David Pavliňák,[d] Jan Přikryl,[a] Ludek Hromadko, [ac] Hanna Sopha, [ac] Josef Krýsa, [b] and Jan M. Macak [*ac]

[a] Center of Materials and Nanotechnologies, Faculty of Chemical Technology, University of Pardubice, Nam. Cs. Legii 565, 53002 Pardubice, Czech Republic

[b] Department of Inorganic Technology, University of Chemistry and Technology Prague, Technicka 5, 16628 Prague, Czech Republic

[c] Central European Institute of Technology, Brno University of Technology, Purkynova 123, 61200 Brno, Czech Republic

[d] Department of Physical Electronics, Masaryk University, Kotlarska 2, 61137 Brno, Czech Republic

Experimental Section

Two different kinds of TiO_2 nanotube layers (TNT layers) were prepared via electrochemical anodization of Ti foils. Prior to all anodizations, Ti foils were degreased by sonication in isopropanol, acetone, isopropanol and dried by a nitrogen jet, respectively. For liquid phase photocatalysis, to obtain ~5 μm thick self-aligned TNTs (2.25 cm^2 area) with a diameter of ~230 nm, anodization of Ti foils (Sigma-Aldrich, 0.127 mm thick, 99.7 % purity) was conducted as previously reported.[1] Briefly, clean Ti foils were anodized at 18 °C using a high-voltage potentiostat (PGU-200V, Elektroniklabor GmbH) in ethylene glycol based electrolyte containing 10 % water and 0.15 M NH_4F at 100 V for 4 h in a two-electrode configuration using Ti foil as a working electrode and Pt foil as a counter electrode. For gas phase photocatalysis, we could not prepare the same type of the TNT layers on the area of 50 cm^2. The development of the process-conditions has not gone so far yet to enable the use of high anodization potentials (e.g. 100 V) needed for larger inner nanotube diameters. This issue was resolved herein by an appropriate cooling of the electrolyte and the use of moderate anodization voltages. The Ti foils were anodized in cooled (18 °C) glycerol based electrolyte containing 50 % water and 0.27 M NH_4F at 20 V for 1 h using a high-voltage potentiostat (PGU-200V, Elektroniklabor GmbH) in a two-electrode configuration using a Pt foil as a counter electrode. The resulting TNTs on large area (50 cm^2) had diameter ~45 nm and average thickness ~1 μm and were prepared using Ti foils (Sigma-Aldrich, 0.127 mm thick, 99.7 % purity) as a starting substrate. After anodization, the TNT layers were sonicated in isopropanol and dried in air, respectively. To obtain anatase structure, the as-prepared amorphous TNT layers were annealed in a muffle oven at 400 °C for 1 h.[2]

The deposition of MoS_2 within the different TNT layers was carried out via Atomic Layer Deposition (ALD, Beneq TFS-200). Bis(t-butylimido)bis(dimethylamino)molybdenum (Strem Chemicals, 98% purity) and hydrogen sulfide (99.5% purity) were used as molybdenum and sulphur precursors, respectively. The MoS_2 was deposited within TNT layers by applying different numbers of ALD cycles i.e. 1, 2, and 5 cycles. These cycle numbers were selected to provide ultrathin nanosheets with a theoretical number of layers (S-Mo-S stacks) corresponding to the ALD cycles (i.e. 1, 2 and 5). All processes were carried out at a temperature of 275 ^{o}C, and using N_2 (99.9999 %) as carrier gas at a flow rate of 500 standard cubic centimeters per minute (sccm). The molybdenum precursor was heated up to 75 ^{o}C to increase its vapour pressure. Under these deposition conditions, one growth ALD cycle was defined by the following sequence: Bis(t-butylimido)bis(dimethylamino) molybdenum pulse (2 s) - Bis(t-butylimido)bis(dimethylamino) molybdenum exposure (45 s) - N_2 purge (90 s) - H_2S pulse (1.75 s) - H_2S exposure (45 s) - N_2 purge (90 s).

The structural and morphological features of blank and MoS_2 decorated TNT layers were characterized by FE-SEM (JEOL, JSM 7500 F) and a high-resolution transmission electron microscope (FEI Titan Themis 60-300, operated at 60keV) equipped with a high angle annular dark field detector for scanning transmission electron microscopy (HAADF-STEM) and SUPER-X energy dispersive X-ray (EDX) spectrometer with 4x30 mm^2 windowless silicon drift detectors. Cross section views were obtained from mechanically bent TNT layers. The X-ray diffraction (XRD) patterns were measured on Panalytical Empyrean diffractometer using Cu X-ray tube and a scintilation detector Pixcel^{3D}. The measurement were performed in the 2θ range 10-40°, the step size was 0.026°. Raman spectra were recorded by LabRAM HR (Horiba Jobin Yvon) and acquired in a continuous scanning mode under a laser excitation wavelength of 532 nm in the range of 100-500 cm^{-1}, grating 800 gr/mm, acquisition set-up 3x100s, 100x objective and 100% ND filter. The composition was monitored by X-ray photoelectron spectroscopy (XPS) (ESCA2SR, Scienta-Omicron) using a monochromatic Al Kα (1486.7 eV) X-ray source. The binding energy scale was referenced to adventitious carbon (284.8 eV). The quantitative analysis was performed using the elemental sensitivity factors provided by the manufacturer. The photocurrent measurements of TNT layers were carried out in an aqueous 0.1 M Na_2SO_4 at 0.4 $V_{vs.Ag/AgCl}$ in the spectral range from 310 to 800 nm. A photoelectric spectrophotometer (Instytut Fotonowy) with a 150 W Xe lamp and a monochromator with a bandwidth of 10 nm connected with a modular electrochemical system AUTOLAB (PGSTAT 204; MetrohmAutolab B. V.; Nova 1.10 software) was used for the photocurrent measurements. Photocurrent stability tests were carried out by measuring the photocurrent produced under chopped light irradiation (light/dark cycles of 10s).

The diffuse reflectance UV-VIS spectra of TNT layers were recorded in the wavelength range from 250 nm to 1 000 nm, using UV-3600Plus Series spectrophotometer (Shimadzu) with ISR-603 integrating sphere.

For the liquid phase photocatalysis, the photocatalytic degradation activities of all samples were evaluated using photodegradation of methylene blue solution (MB, initial concentration 1 x 10^{-5} M). Prior to all measurements, to achieve a

dye adosrption/desorption equilibrium, the samples were immersed in 3.5 mL of the MB solution for 60 min with constant stirring. Afterwards, the samples were irradiated by a LED-based UV lamp (10 W, λ=365 nm ± 5 nm) and VIS lamp (10 W λ=410-425 nm), and the absorbance of the MB solution was periodically measured (10 or 30 min steps) by a UV-VIS spectrometer (S-200, Boeco) at a wavelength of 670 nm to monitor the degradation rates.

For the gas phase photocatalysis, as previously reported[3], the photocatalytic setup was realised according to the ISO 22197-2 specifications and irradiated under a UV lamp (1 mW/cm^2, λ_{max}=351 nm) using hexane as a model aliphatic compound. Compared to the standard ISO 22197 specification, the acetaldehyde is replaced by hexane, which is more difficult to decompose. Briefly, a calibrated gas mixture composed of 100 ppm hexane in N_2 was used as the pollutant source (Linde Gas) which was further diluted with humidified air to a final mixture of 5 ppm hexane in air that was admitted to the reactor with a flow rate of 0.5 dm^3/min. The relative humidity in the reactor was set to 50%. Analysis of the gaseous mixture was performed by GC-FID (Varian CP-3800) with capillary column CP-Sil 5 CB 15x0.25 (0.25) and flame ionization detector. The active photocatalyst area was 50 cm^2 and the distance of the glass cover was 0.5 cm.

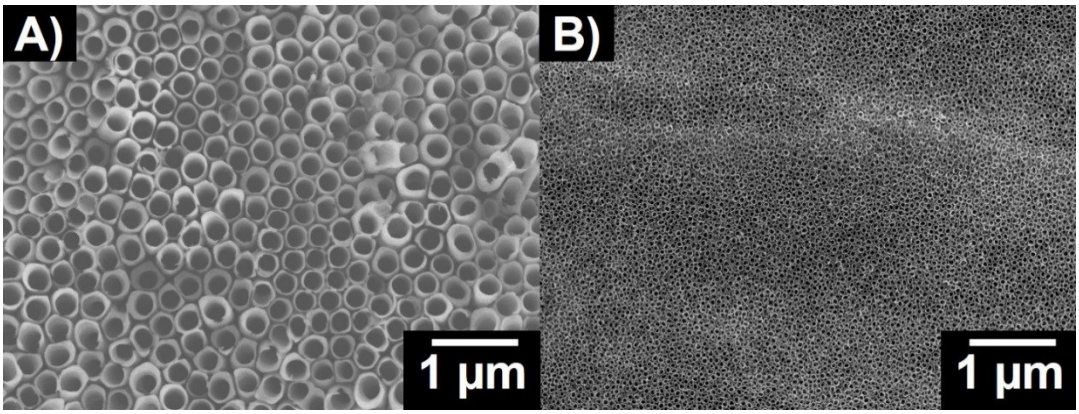

Figure S1 Low magnification top-view SEM images of (A) ~5 µm and (B) ~1 µm thick TNT layers, respectively. The nanotubes layers have significanly different average inner nanotube diameter of (A) ~230 nm and (B) ~45 nm. However, their aspect ratio (i.e. the ratio between the nanotube layer thickness and the inner diameter) is for both layers approx. 22.

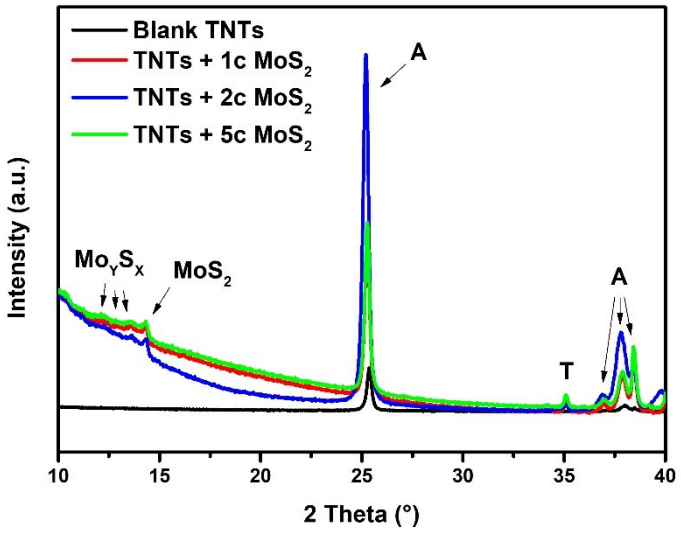

Figure S2 XRD patterns of blank blank and MoS_2 decorated 5 µm thick TNT layers. A – anatase TiO_2; T – titanium.

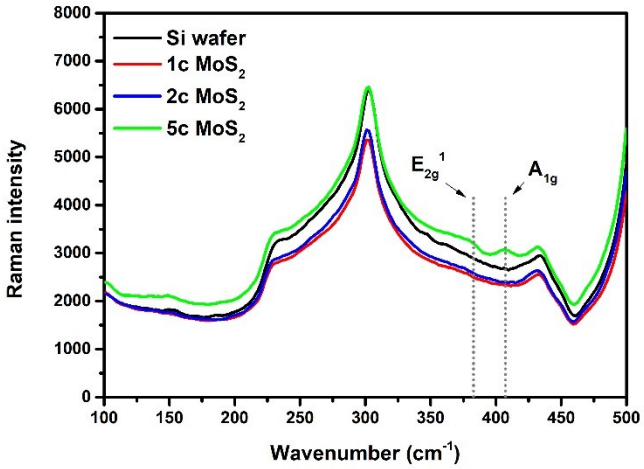

Figure S3 Raman spectra of 1, 2 and 5 MoS_2 ALD cycles decorated Si wafer.

The 1, 2 and 5 MoS_2 ALD cycles decorated Si wafer (with a native SiO_2 thin layer on it) was characterized using micro-Raman spectroscopy. In the case of MoS_2, two principal peaks are expected at ~384 cm^{-1} and 403 cm^{-1}, corresponding to $E_{2g}{}^1$ and A_{1g} modes, respectively. The other strong E_{1g} vibration mode at ~286 cm^{-1} cannot be observed in our case due to the use of optical pathway of microscope and back scattering configuration of laser beam. No signals for 1 and 2 MoS_2 ALD cycles were obtained. However, for 5 MoS_2 ALD cycles a clear signal of MoS_2 with the major signal at ~406 cm^{-1} and 382cm^{-1}, corresponding to $E_{2g}{}^1$ and A_{1g} modes respectively, is present. The presence of MoS_2 can be detected only on samples with higher number of ALD cycles due to the fact that these signals overlap with signals naturally occuring on Si and Ti.

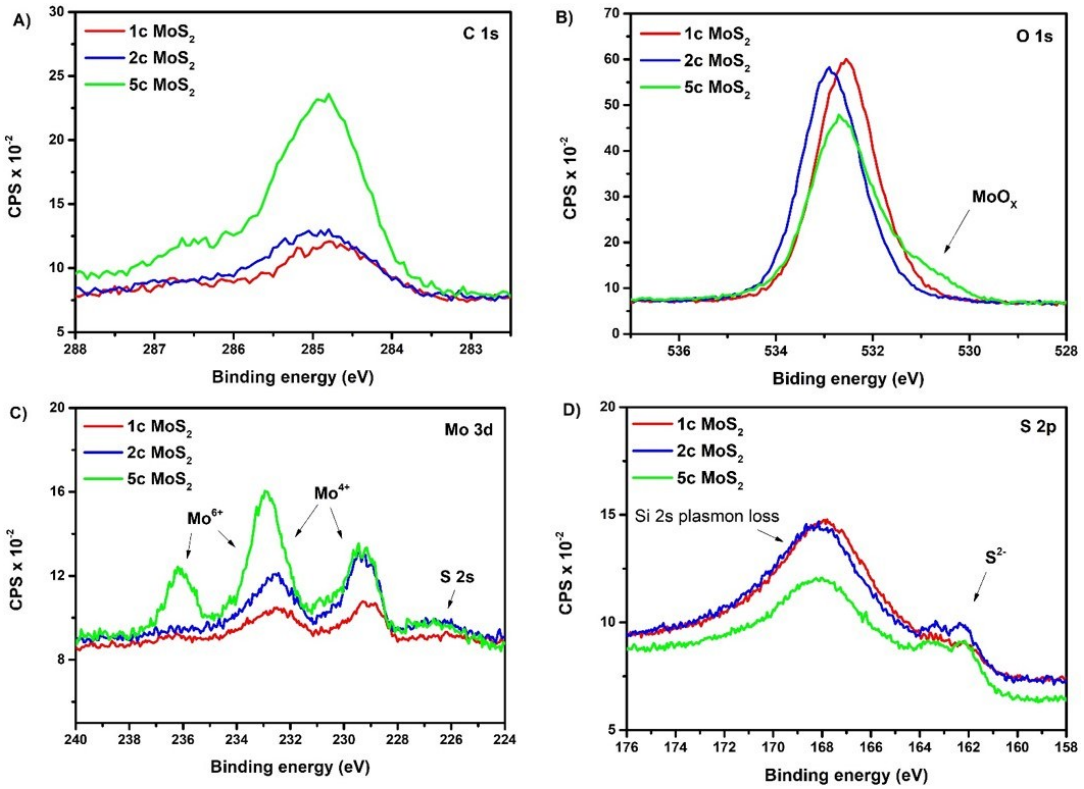

Figure S4 High-resolution XPS spectra of (A) C 1s, (B) O 1s, (C) Mo 3d, and (D) S 2p for 1, 2 and 5 MoS_2 ALD cycles on Si wafers.

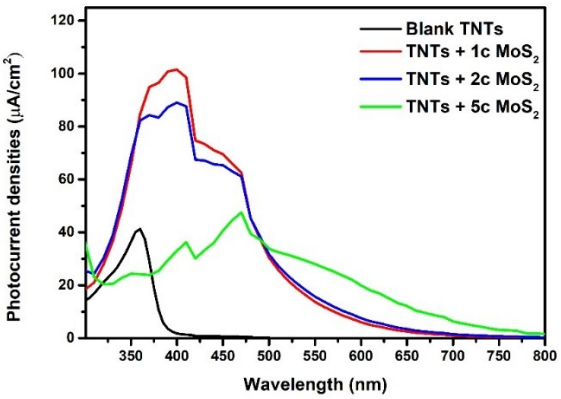

Figure S5 Photocurrent densities recorded for blank and MoS_2 decorated 5 µm thick TNT layers. The „*X*c" specifies the number of MoS_2 ALD cycles.

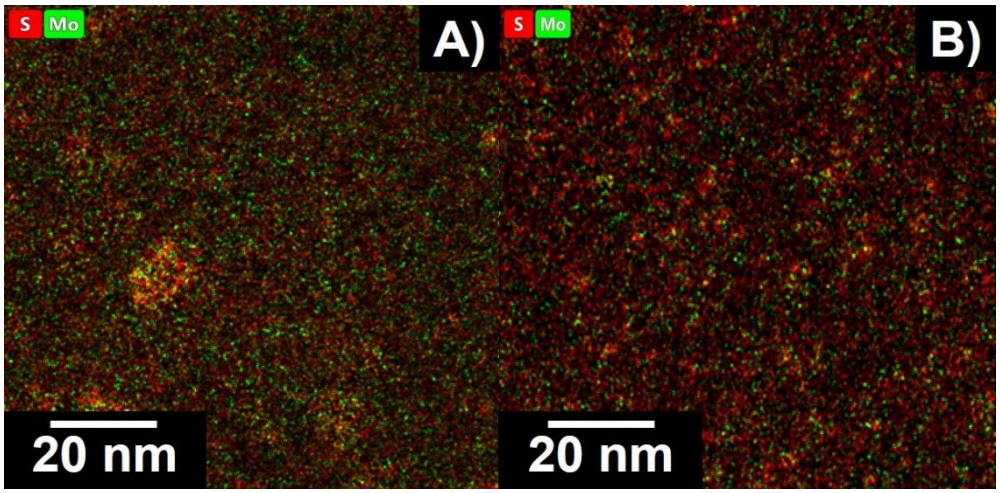

Figure S6 Planar view in STEM HAAD image and corresponding STEM EDX elemental maps revealing MoS_2 decoration in form of nanosheets and their density on nanotube walls after (A) 2 and (B) 5 MoS_2 ALD cycles.

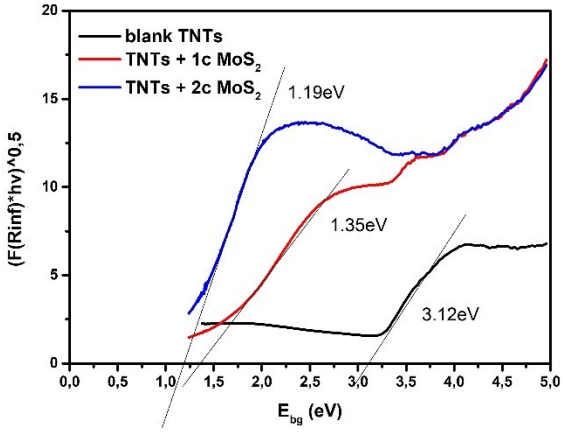

Figure S7 Evaluation of the optical band gap of blank and MoS_2 decorated TNT layers using Kubelka-Munk function.

Mechanism of the liquid phase photodegradation on the MoS_2/TiO_2 interface

Due to quantum confinement effect of nanoscale MoS_2, the conduction band (CB) level of MoS_2 is more negative than that of anatase TiO_2. The valence band (VB) level of anatase TiO_2 is more positive than that of MoS_2.[4–6] Based on the energy band characteristics of MoS_2 and anatase TiO_2, the photocatalytic mechanisms and charge transfer mechanisms in the MoS_2/TiO_2 are following. Under light irradiation, electron/hole (e^-/h^+) pairs are generated and the photogenerated e^- in the CB of TiO_2 exhibits enough redox potential to produce hydrogen or oxygen molecules to form superoxide anion radicals. Such radicals are powerful and nonselective oxidants, and can completely degrade almost all organic pollutants.[6] Simultaneously, the photogenerated h^+ move toward the opposite direction and participate in the dye photodegradation proces directly in the VB of MoS_2. Moreover, the photogenerated charge carrier transfer and separation is facilitated by the inner electric field in the heterojunction.[4–6] In such way, the photons are effectively harvested and utilized.

Mechanism of hexane-to-CO_2 conversion

Kinetics of the photocatalytic removal of hexane was described in previous work[7] for the initial hexane concentrations ranging from 70 to 3800 ppm. The correlation between the amount of photocatalytically removed hexane and produced CO_2 suggests that the hexane is converted to a significant extent to CO_2.

A more detailed study[8] on the mechanism of photocatalytic hexane removal shows that after 23 min of UV irradiation in the close loop reactor, the hexane-to-CO_2 conversion was 53%. After 40 min of this irradiation, the concentration of produced CO_2 further increased to 98%. Based on these results, the conversion of hexane and all its by-products to CO_2 on the time scale used in this work (60 minutes) can be expected. Two possible pathwas can be put forward for the photocatalytic hexane removal, according to results from mass spectroscopy: 1) formation of an organic radical by the abstraction of hydrogen atoms from the hexane structure by •OH and subsequent reaction with O_2 to form $\bullet O_2^{2-}$ which further oxidizes to ketone. 2) abstraction of hydrogen atoms and subsequent reaction with •OH to form secondary alcohols. The main by-products were identified as 2-hexanol, 3-hexanol and appropriate ketones, such as 2(3)-hexanone.

References:

1 S. Das, H. Sopha, M. Krbal, R. Zazpe, V. Podzemna, J. Prikryl and J. M. Macak, *ChemElectroChem*, 2017, **4**, 495–499.

2 S. Das, R. Zazpe, J. Prikryl, P. Knotek, M. Krbal, H. Sopha, V. Podzemna and J. M. Macak, *Electrochim. Acta*, 2016, **213**, 452–459.

3 H. Sopha, M. Baudys, M. Krbal, R. Zazpe, J. Prikryl, J. Krysa and J. M. Macak, *Electrochem. commun.*, 2018, **97**, 91–95.

4 M. Sabarinathan, S. Harish, J. Archana, M. Navaneethan, H. Ikeda and Y. Hayakawa, *RSC Adv.*, 2017, **7**, 24754–24763.

5 Z. Li, X. Meng and Z. Zhang, *J. Photochem. Photobiol. C Photochem. Rev.*, 2018, **35**, 39–55.

6 Y. Lin, P. Ren and C. Wei, *CrystEngComm*, 2019, **21**, 3439–3450.

7 F. Moulis and J. Krýsa, *Catal. Today*, 2013, **209**, 153–158.

8 J. O. Saucedo-Lucero and S. Arriaga, *Chem. Eng. J.*, 2013, **218**, 358–367.